Electronic Supplementary Material (ESI) for Energy & Environmental Science.
This journal is © The Royal Society of Chemistry 2022

# Supporting Information

## Interfacial Effect induced by Rare Earth Oxide in Boosting Conversion of $CO_2$ to Formate

*Lianpeng Song, Zhong Liang, Mingzi Sun, Bolong Huang*, Yaping Du**

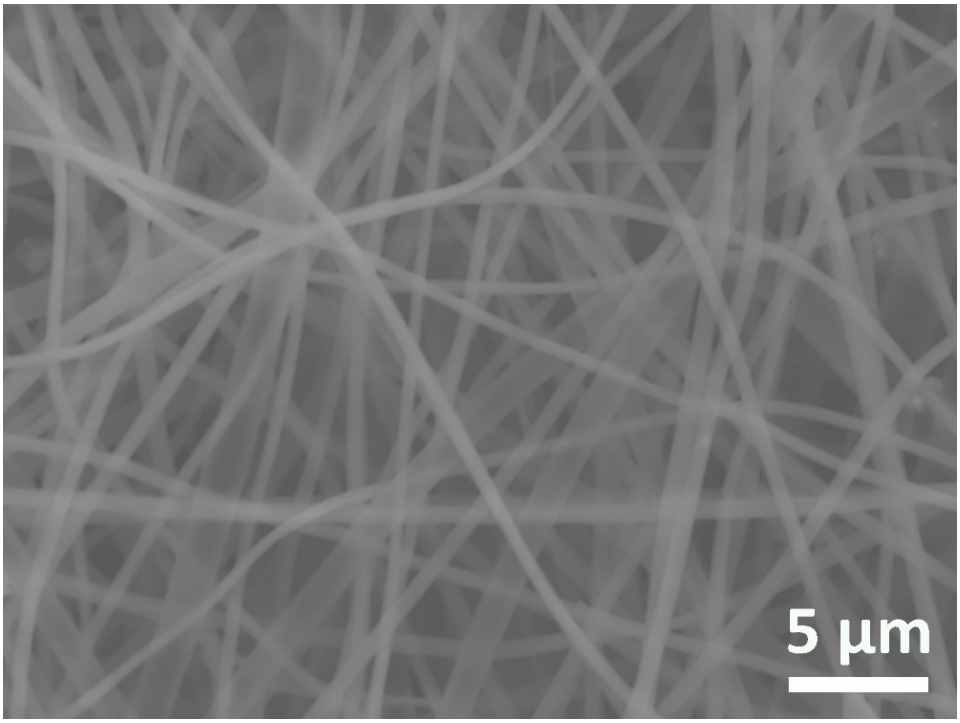


**Fig. S1** SEM image of as-spun fiber of $CeO_2/Bi_3NbO_7$.

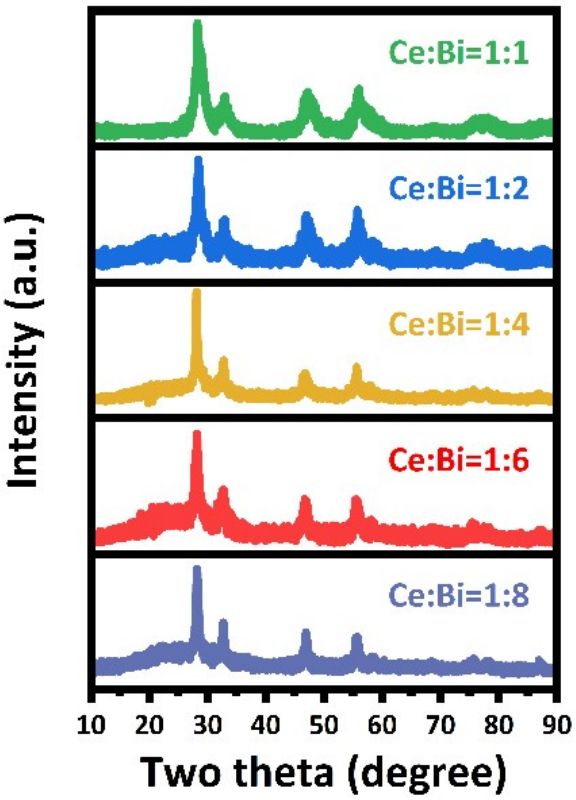


**Fig. S2** XRD pattern comparison of $CeO_2/Bi_3NbO_7$ with different Ce: Bi ratios.

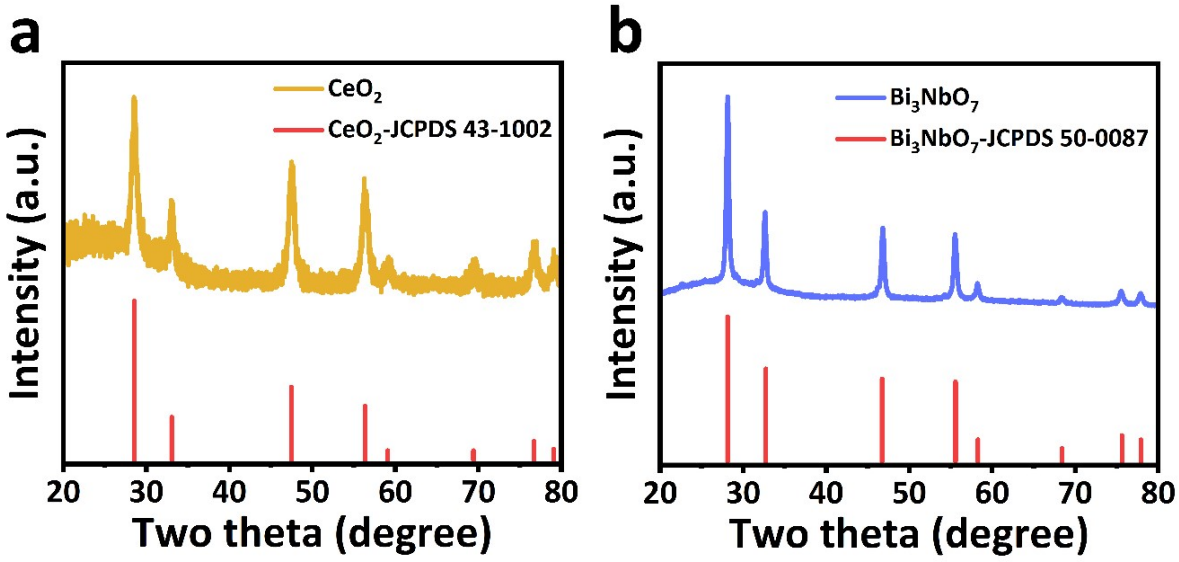


**Fig. S3 a** XRD pattern of $CeO_2$ and **b** $Bi_3NbO_7$.

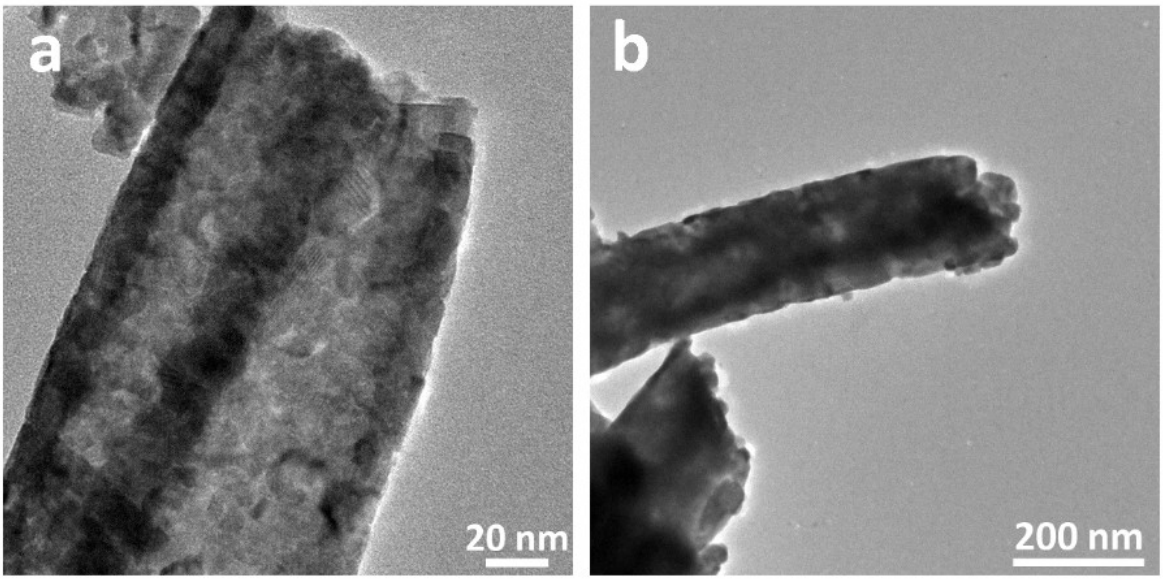


**Fig. S4** Morphologic characterization of **a** $CeO_2$ and **b** $Bi_3NbO_7$

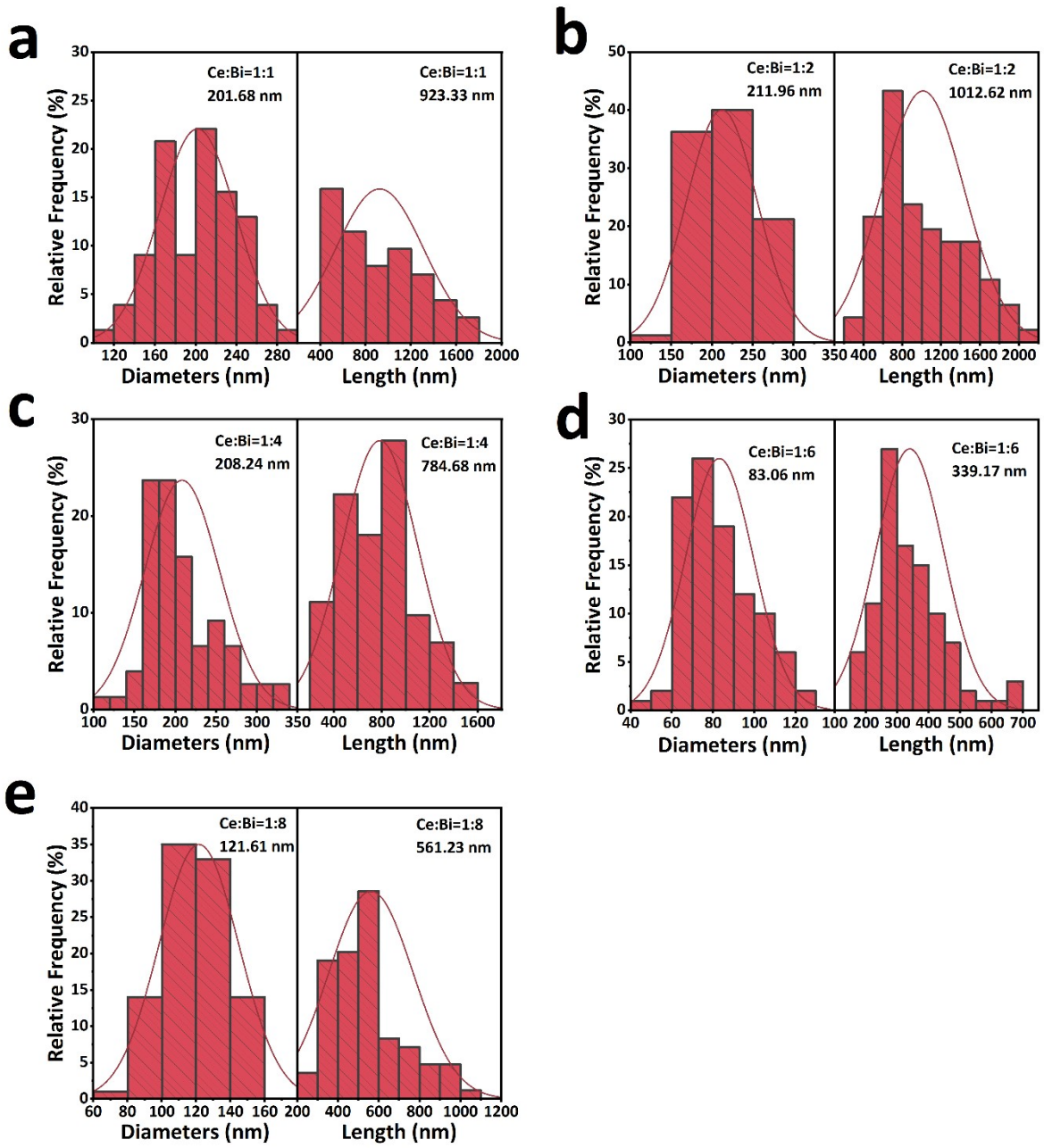


**Fig. S5** The comparisons of the size distributions (diameters and length) for $CeO_2/Bi_3NbO_7$ with different ratios.

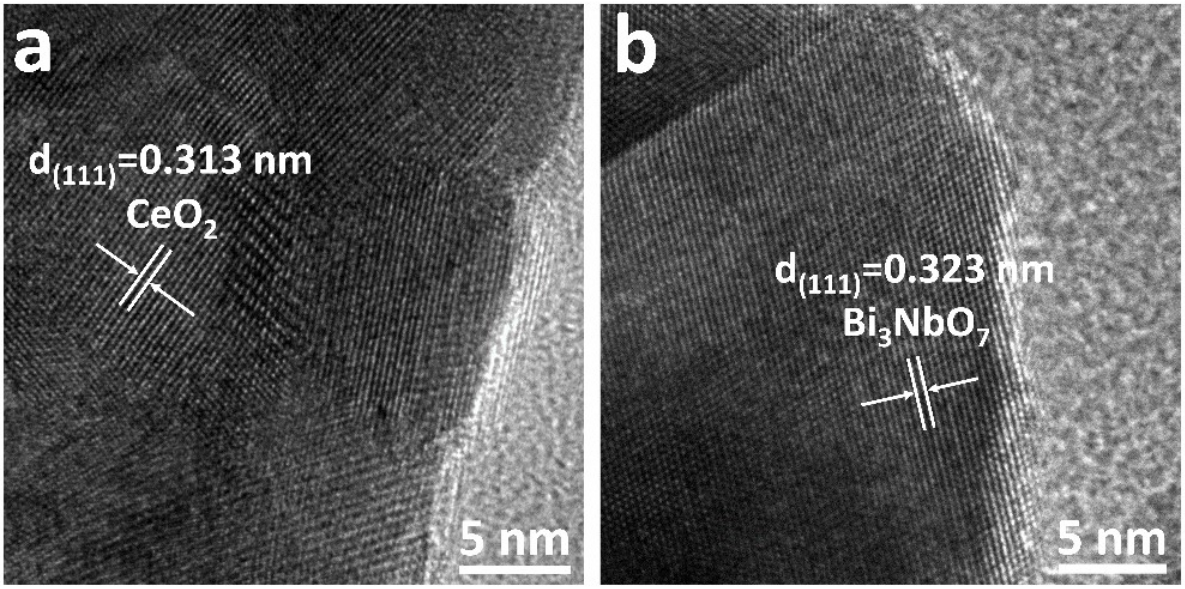


**Fig. S6** HRTEM images of **a** $CeO_2$ and **b** $Bi_3NbO_7$.

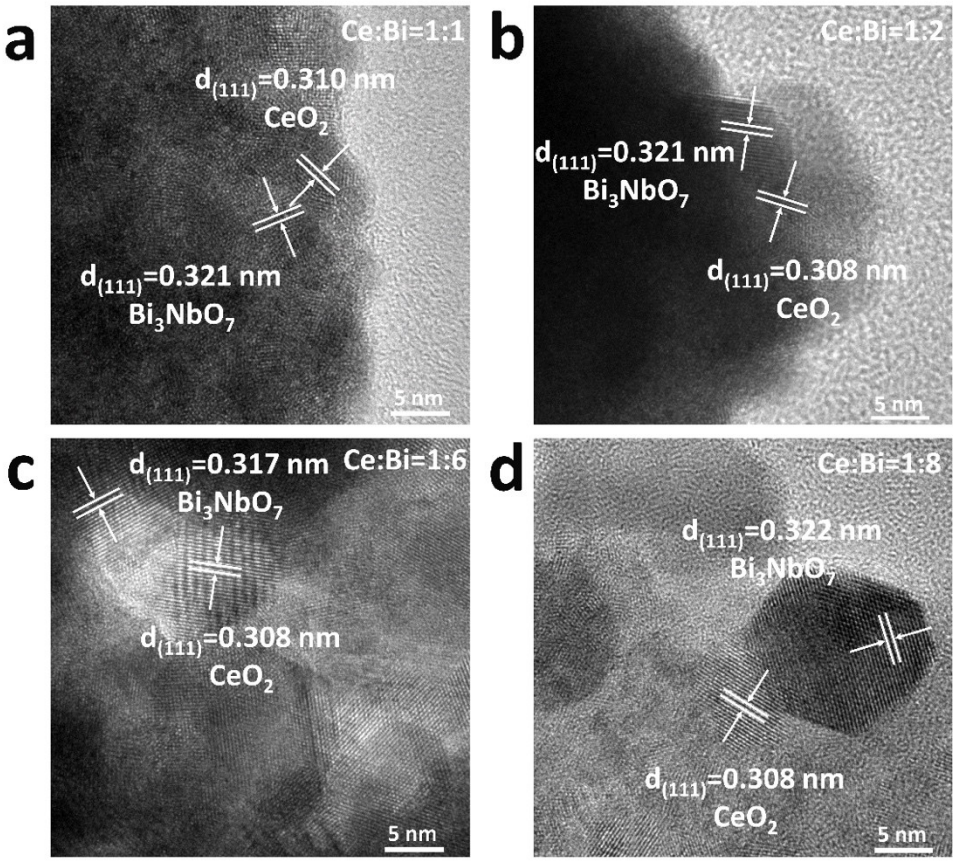


**Fig. S7** HRTEM of the interfaces in $CeO_2/Bi_3NbO_7$ with different Ce: Bi ratios.

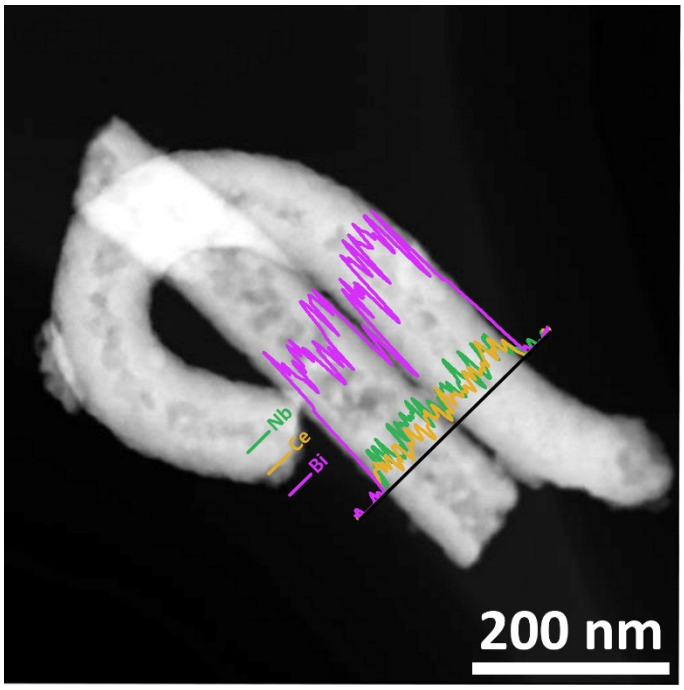


**Fig. S8** The line scan of different elements of $CeO_2/Bi_3NbO_7$.

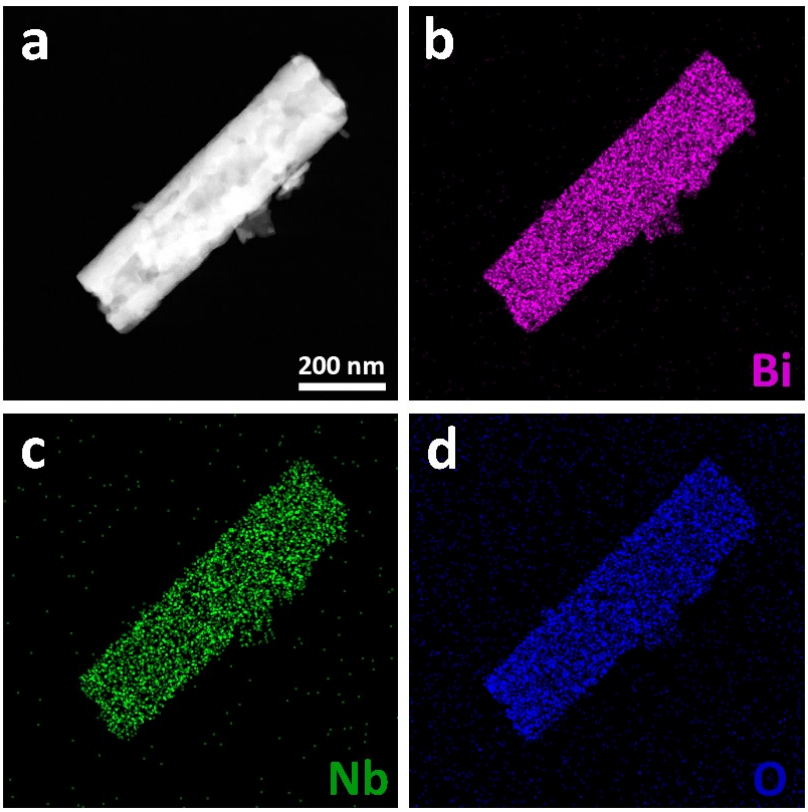


**Fig. S9 a-d** Corresponding elemental mapping images of $Bi_3NbO_7$.

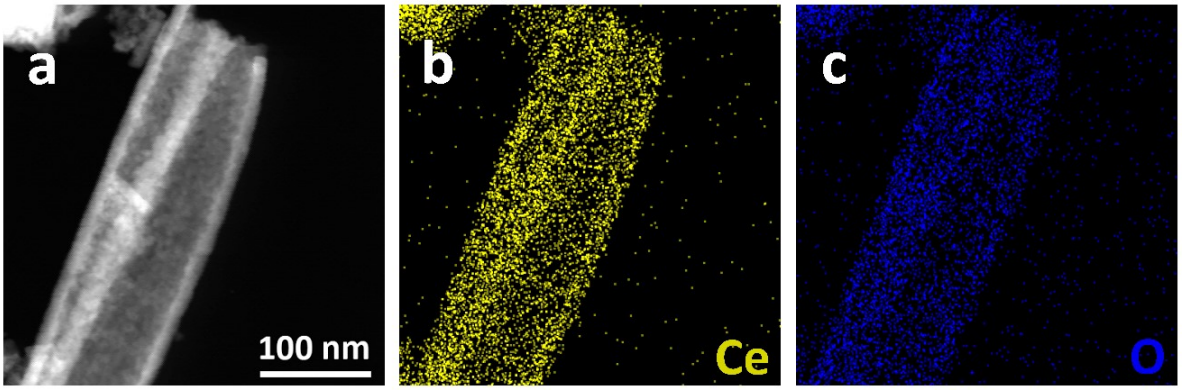


**Fig. S10** a-c Corresponding elemental mapping images of $CeO_2$.

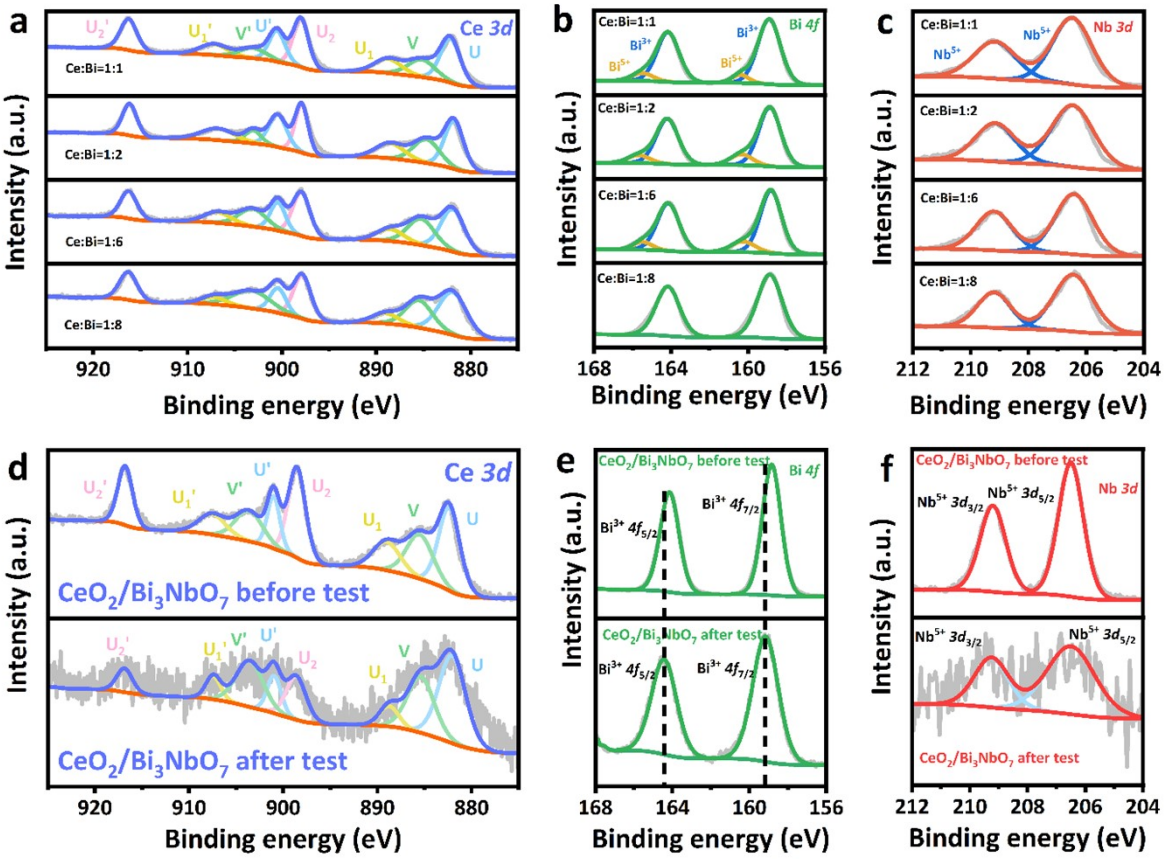


**Fig. S11. a-c** XPS of $CeO_2/Bi_3NbO_7$ with different ratios. **d-f** XPS of $CeO_2/Bi_3NbO_7$ before and after tests.

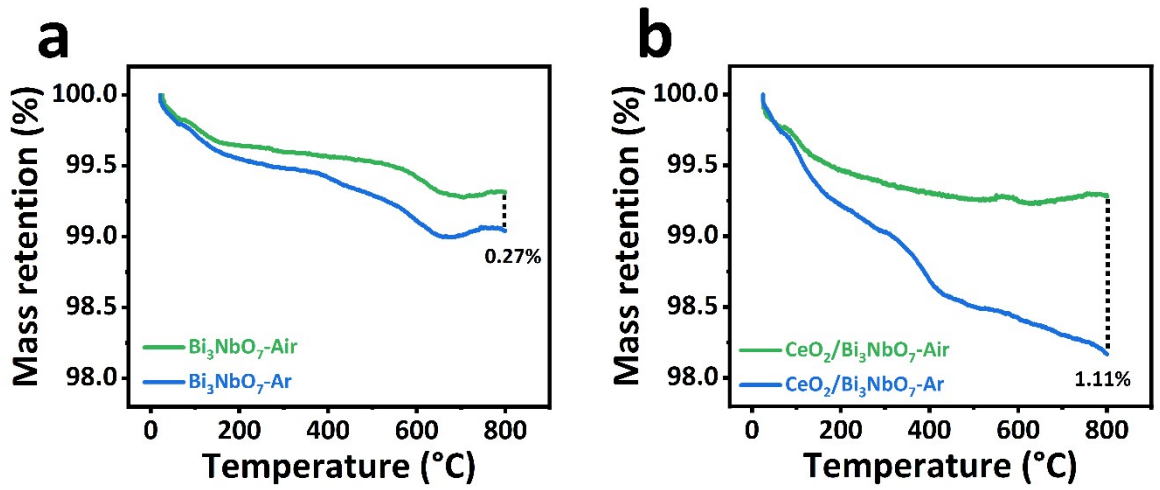


**Fig. S12. a-b** TGA analysis of $Bi_3NbO_7$ and $CeO_2/Bi_3NbO_7$ in air and argon atmosphere. (Flow of 100 mL/min and a ramping rate of 10 °C/min). The concentration of oxygen vacancies was calculated from the difference in weight decrease between the two TGA traces.

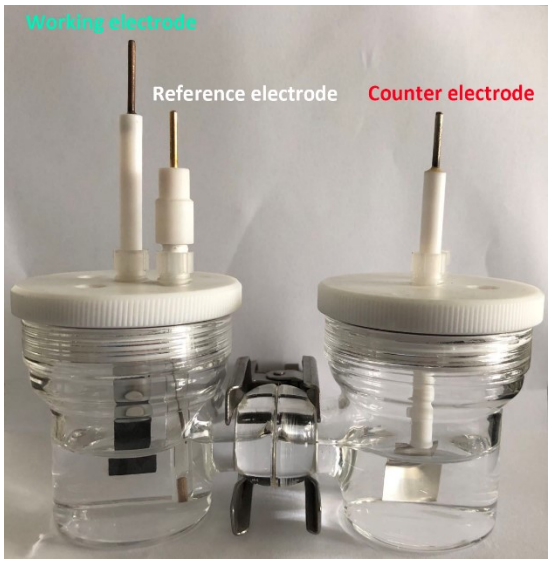


**Fig. S13** H-type cell for electrocatalytic carbon dioxide reduction.

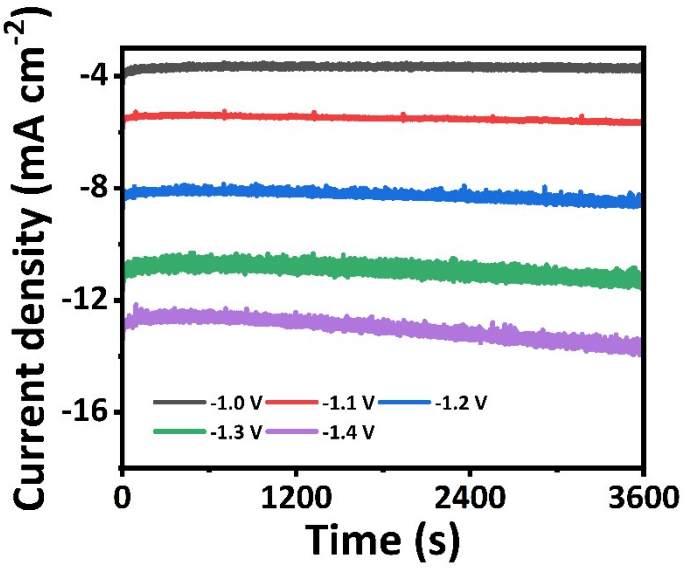


**Fig. S14** Chronoamperometric curves of $CeO_2/Bi_3NbO_7$ (1: 4) at different working potentials.

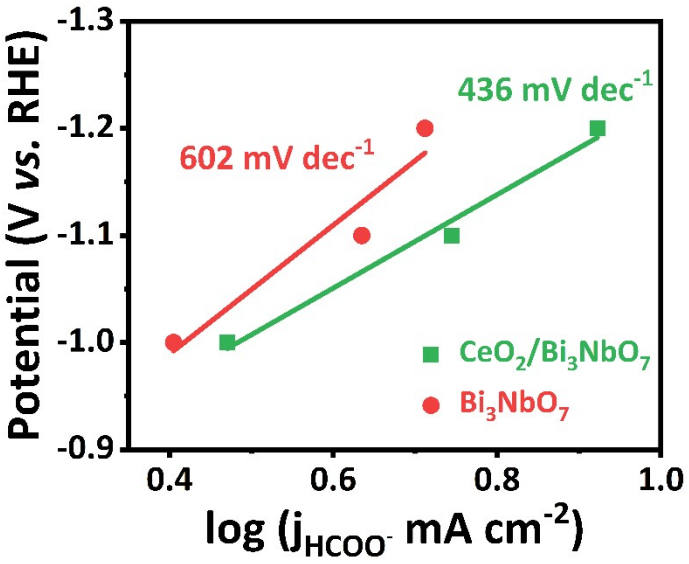


**Fig. S15** Tafel plot of $Bi_3NbO_7$ and $CeO_2/Bi_3NbO_7$.

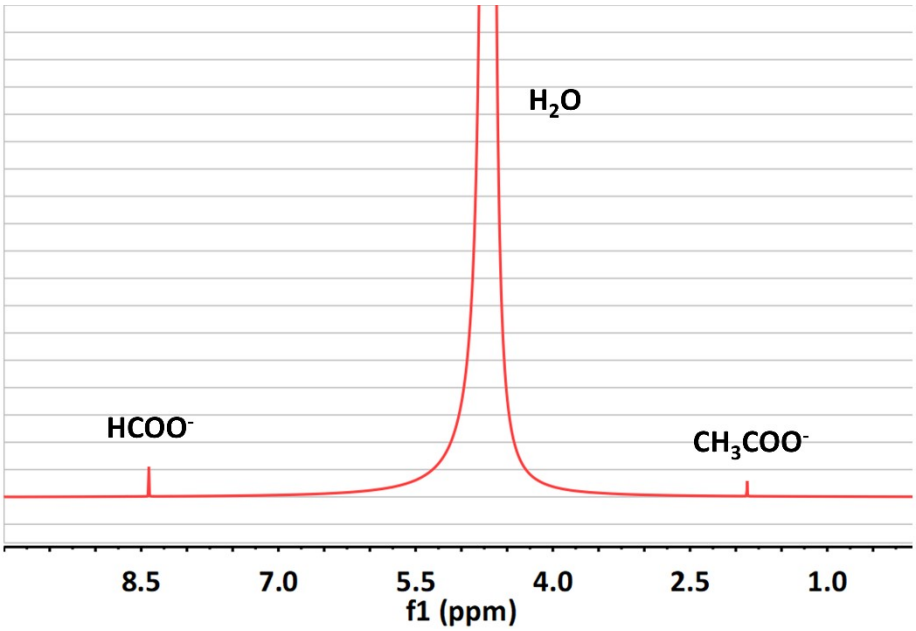


**Fig. S16** Representative NMR spectrum of $CeO_2/Bi_3NbO_7$ after electrolysis at -1.2 V versus RHE for 6 h.

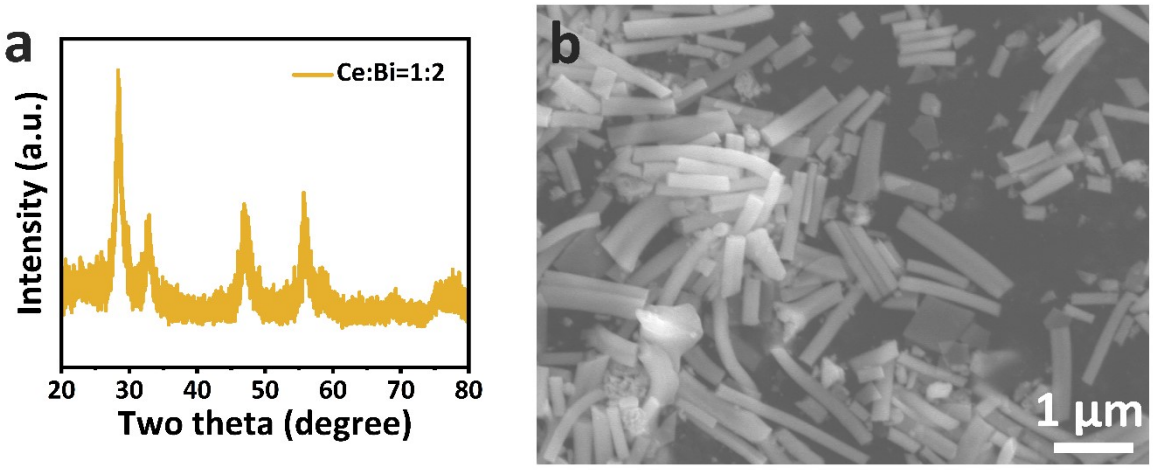


**Fig. S17 a** XRD pattern, **b** SEM image of the complex with a molar ratio of Ce and Bi of 2.

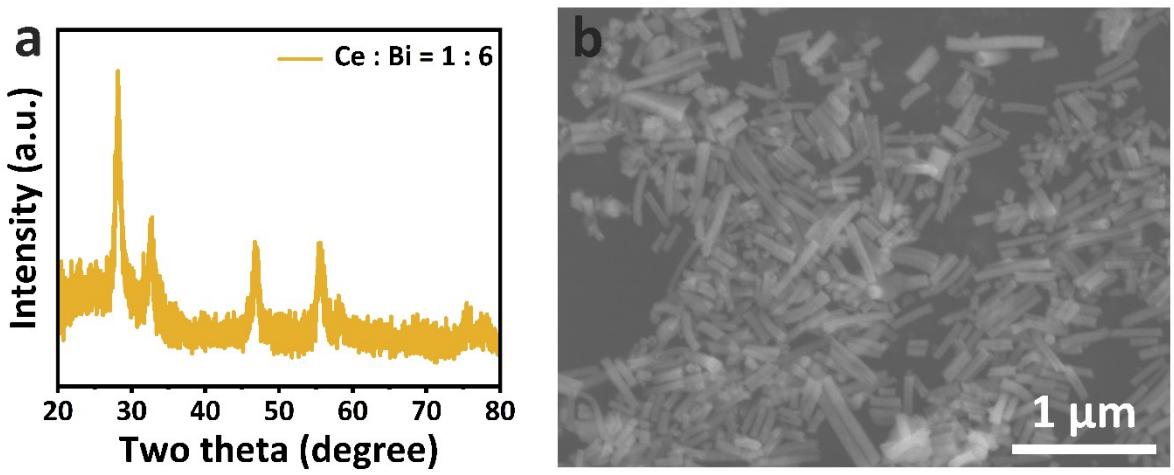


**Fig. S18 a** XRD pattern, **b** SEM image of complex with a molar ratio of Ce and Bi of 6.

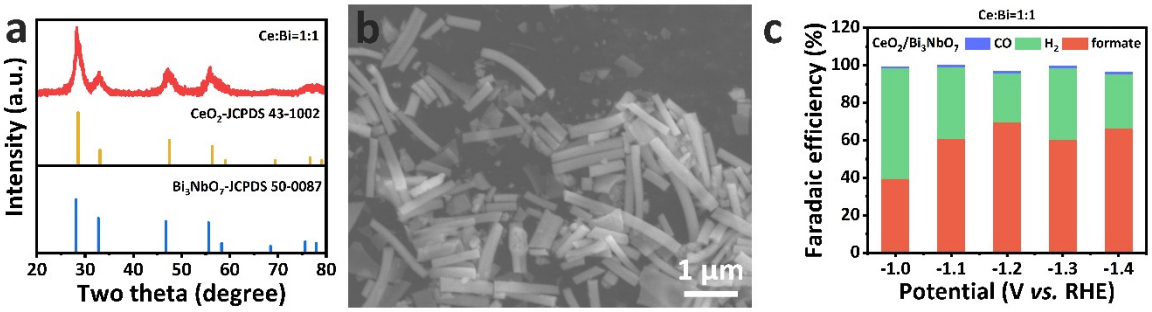


**Fig. S19 a** XRD pattern, **b** SEM image and c FE of formate, $CO_2$ and $H_2$ of $CeO_2/Bi_3NbO_7$ (Ce/Bi=1/1) at selected voltages.

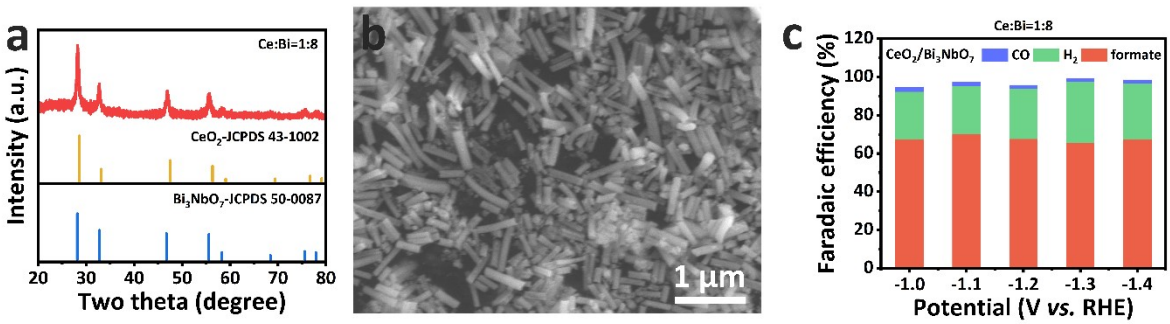


**Fig. S20 a** XRD pattern, **b** SEM image and **c** FE of formate, $CO_2$ and $H_2$ of $CeO_2/Bi_3NbO_7$ (Ce/Bi=1/8) at selected voltages.

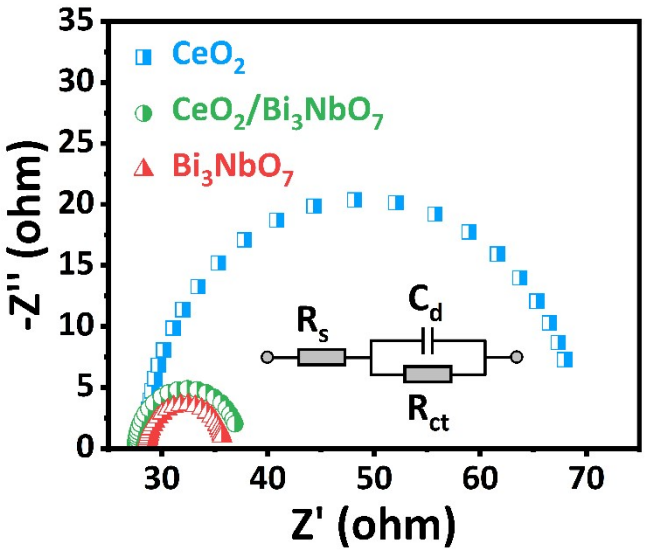


**Fig. S21** Electrochemical impedance spectra (EIS) of $CeO_2$, $Bi_3NbO_7$ and $CeO_2/Bi_3NbO_7$ at -1.2 V versus RHE, after fitting.

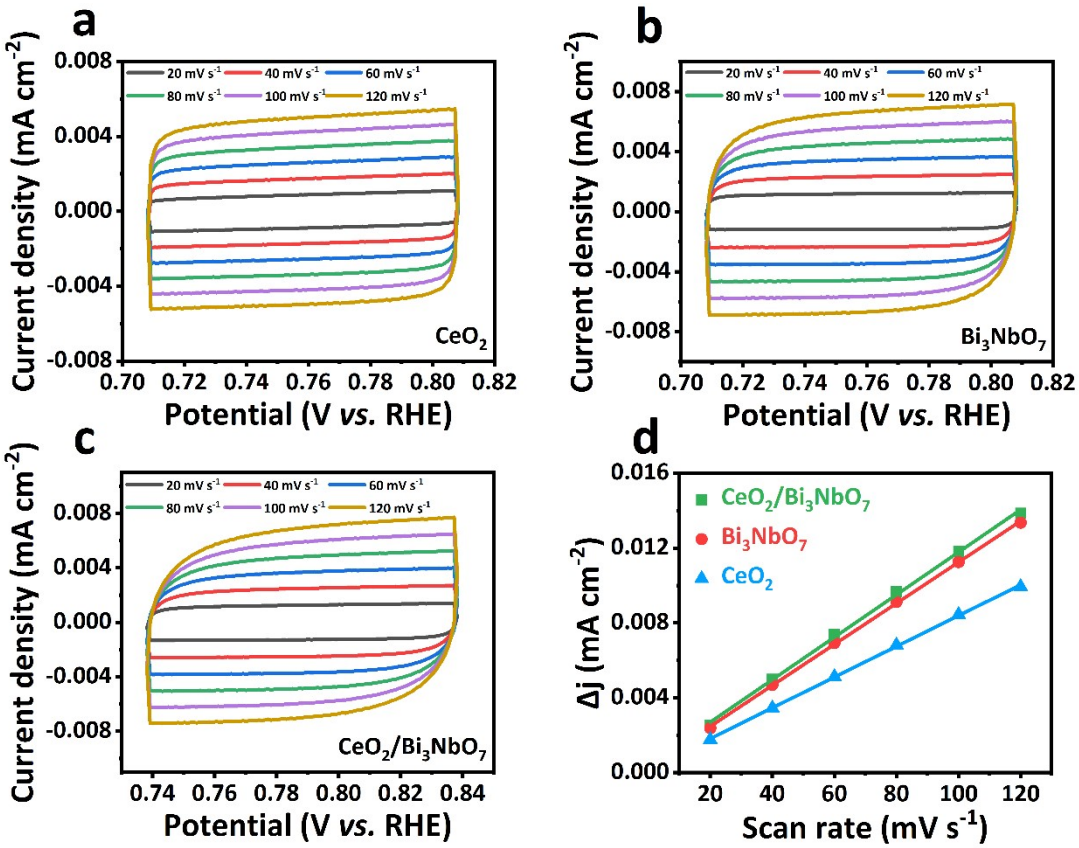


**Fig. S22** Cyclic voltammetry curves of a $CeO_2$, b $Bi_3NbO_7$, c $CeO_2/Bi_3NbO_7$ and d different samples plotted against scan rate.

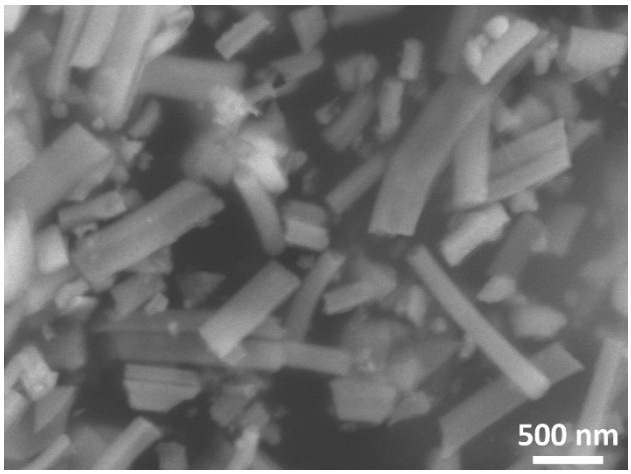


**Fig. S23** SEM images of the $CeO_2/Bi_3NbO_7$ dispersed on carbon paper after 12 h stability test.

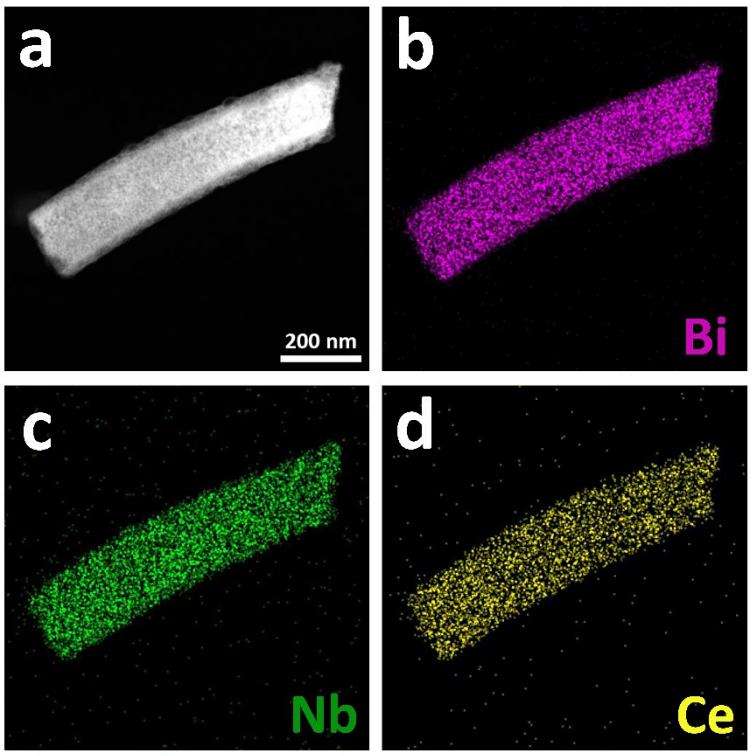


**Fig. S24 a-d** Corresponding elemental mapping images of $CeO_2/Bi_3NbO_7$ after stability test.

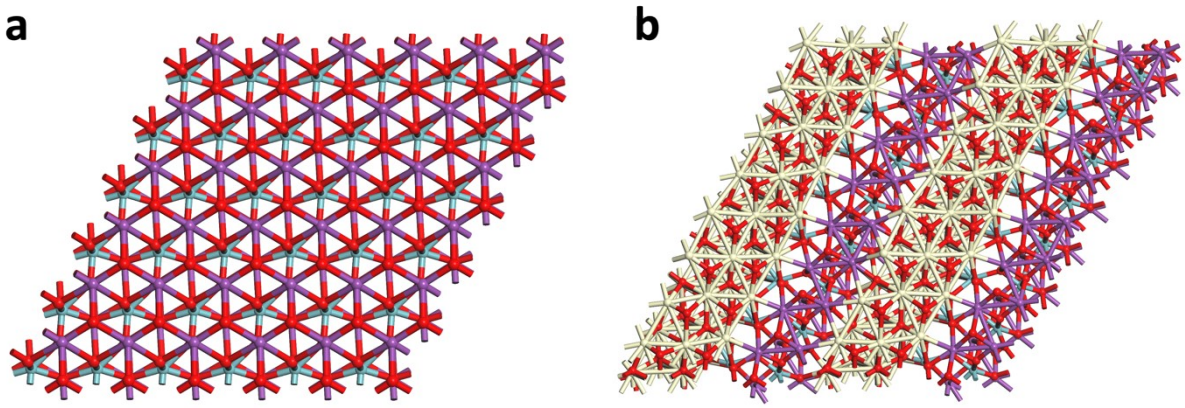


**Fig. S25** The DFT calculation models of (a) $Bi_3NbO_7$ and (b) $CeO_2/Bi_3NbO_7$ after relaxation.

**Table S1.** The morphology analysis of different $CeO_2/Bi_3NbO_7$ samples.

| Ce: Bi Ratio Sample | diameters (nm) | Length (nm) |
|---|---|---|
| 1:1 | 201.68 | 923.33 |
| 1:2 | 211.96 | 1012.62 |
| 1:4 | 208.24 | 784.68 |
| 1:6 | 83.06 | 339.17 |
| 1:8 | 121.61 | 561.23 |

**Table S2.** The composition ratios of different $CeO_2/Bi_3NbO_7$ samples.

| Ce: Bi Ratio Sample | Ce Ratio (%) | Bi Ratio (%) | Nb Ratio (%) |
|---|---|---|---|
| 1:1 | 41.01 | 42.23 | 16.76 |
| 1:2 | 26.26 | 55.52 | 18.22 |
| 1:4 | 17.61 | 60.06 | 22.33 |
| 1:6 | 13.11 | 63.48 | 23.41 |
| 1:8 | 9.22 | 72.67 | 18.11 |

**Table S3.** Performance comparison of $CeO_2/Bi_3NbO_7$ with other Bi-based electrocatalysts reported recently.

| Catalysts | Electrolyte | Formate FE | $j_{formate}$ | Ref. |
|---|---|---|---|---|
| 2.0 M $KHCO_3$ | Bi@Sn NPs | 92%@-1.0 V *vs.* RHE | 230 mA $cm^{-2}$ | 1 |
| 0.1 M $KHCO_3$ | Ag - Bi | 88.4%@-1.2 V *vs.* RHE | 18.74 mA $cm^{-2}$ | 2 |
| 0.1 M $KHCO_3$ | $Bi_2O_2CO_3$ | 83%@-0.59 V *vs.* RHE | 0.17 mA $cm^{-2}$ | 3 |
| 0.1 M $KHCO_3$ | $Bi_{52}Sn_{46}In_2$ | 82%@-1.2 V *vs.* RHE | 25 mA $cm^{-2}$ | 4 |
| 0.1 M $HNO_3$ | MWCNT@$CeO_2$ | 65%@-0.22 V *vs.* RHE | 0.325 mA $cm^{-2}$ | 5 |
| 0.1 M $HNO_3$ | $Bi_xSn_{1-x}$ | 78%@-1.1 V *vs.* RHE | 9.36 mA $cm^{-2}$ | 6 |
| 0.1 M $KHCO_3$ | $CeO_2/Bi_3NbO_7$ | 83.13%@-1.4 V *vs.* RHE | 14.29 mA $cm^{-2}$ | This work |

## Reference


1. Xing, Y.; Kong, X.; Guo, X.; Liu, Y.; Li, Q.; Zhang, Y.; Sheng, Y.; Yang, X.; Geng, Z.; Zeng, J., Bi@Sn Core-Shell Structure with Compressive Strain Boosts the Electroreduction of $CO_2$ into Formic Acid. *Adv. Sci.* 2020, *7* (22), 1902989.

2. Zhou, X.; Lu, X.; Yu, T.; Wang, H.; Qian, L.; Lei, P.; Yu, Y.; Liu, L.; Xia, S.; Fang, J., Conformal Shell Amorphization of Nanoporous Ag-Bi for Efficient Formate Generation. *ACS Appl. Mater. Interfaces* 2020, *12* (28), 31319-31326.

3. Lv, W.; Bei, J.; Zhang, R.; Wang, W.; Kong, F.; Wang, L.; Wang, W., Bi2O2CO3 Nanosheets as Electrocatalysts for Selective Reduction of $CO_2$ to Formate at Low Overpotential. *ACS Omega* 2017, *2* (6), 2561-2567.

4. Allioux, F. M.; Merhebi, S.; Ghasemian, M. B.; Tang, J.; Merenda, A.; Abbasi, R.; Mayyas, M.; Daeneke, T.; O'Mullane, A. P.; Daiyan, R.; Amal, R.; Kalantar-Zadeh, K., Bi-Sn Catalytic Foam Governed by Nanometallurgy of Liquid Metals. *Nano Lett* 2020, *20* (6), 4403-4409.

5. Valenti, G.; Melchionna, M.; Montini, T.; Boni, A.; Nasi, L.; Fonda, E.; Criado, A.; Zitolo, A.; Voci, S.; Bertoni, G.; Bonchio, M.; Fornasiero, P.; Paolucci, F.; Prato, M., Water-Mediated ElectroHydrogenation of $CO_2$ at Near-Equilibrium Potential by Carbon Nanotubes/Cerium Dioxide Nanohybrids. *ACS Appl. Energy Mater.* 2020, *3* (9), 8509-8518.

6. Tang, J.; Daiyan, R.; Ghasemian, M. B.; Idrus-Saidi, S. A.; Zavabeti, A.; Daeneke, T.; Yang, J.; Koshy, P.; Cheong, S.; Tilley, R. D.; Kaner, R. B.; Amal, R.; Kalantar-Zadeh, K., Advantages of eutectic alloys for creating catalysts in the realm of nanotechnology-enabled metallurgy. *Nat. Commun.* 2019, *10* (1), 4645.